Modeling and Optimization of Compact Microwave Bandpass Filters

Maged Bekheit, *Member, IEEE*, Smain Amari, *Member, IEEE*, and Wolfgang Menzel, *Fellow, IEEE*

***Abstract*—This paper presents the modeling and optimization of compact microwave bandpass filters whose compactness leads to complex and strong stray coupling paths, thereby making the identification of a simple and sparse coupling topology difficult and even impossible. The strong coupling coefficients needed for a broadband response can also cause an ambiguity in identifying the spatial extent of local resonances. An equivalent circuit, which is extracted directly from Maxwell's equations, is used in optimizing these filters. The filter is represented by its global resonances instead of individual resonators. The extraction of the parameters of the equivalent circuit is carried out in the physical frequency and not in the normalized frequency in order to preserve the physicality of the equivalent circuit, especially for asymmetric responses. The technique is successfully applied to the optimization of second-order suspended stripline bandpass filters with one transmission zero either below or above the passband, as well as fourth-order filters with three transmission zeros. A fourth-order filter with three transmission zeros is fabricated and measured.**

***Index Terms*—Eigenmode, resonator filters, suspended stripline (SSL), synthesis.**

I. Introduction

MODERN wireless communication systems have increased the demand for compact microwave filters. As the size of these filters is decreased, stray electromagnetic (EM) interactions between their individual building blocks, especially resonators, are increased. Identifying a simple and sparse topology to account for the couplings between the resonators becomes difficult and even impossible. The problem is accentuated in filters with moderate to broad and ultra-wide bandwidths in which strong couplings are needed. An accurate equivalent circuit must account for all these effects in addition to the frequency dependence of the coupling coefficients in simple topologies. Obviously, the coupling matrix concept, which is a narrowband approximation, is not practical in designing these filters.

A narrowband coupled resonator bandpass filter of order N has been thus far modeled as a set of N resonances that are coupled by frequency-independent coupling coefficients. Under the narrowband assumption, the equivalent circuit is the classical coupling matrix whose diagonal elements represent the frequency shifts in the resonant frequencies of the individual resonators with respect to the center of the passband [1]. Its off-diagonal elements are the frequency independent coupling coefficients between the different resonators and between the ports and resonators. A comprehensive solution to the problem of extracting the elements of the coupling matrix with a desired topology to reproduce a prescribed response is now known [2].

The design and optimization of microwave coupled resonator bandpass filters, through space-mapping techniques, for example, assumes a topology that is capable of reproducing the target response including the presence of transmission zeros at finite frequencies. An underlying and crucial assumption of this approach is that the individual resonances and their spatial extent, as well as that the coupling topology can be easily identified. This is certainly the case for most narrowband filters. However, the identification of a simple and sparse coupling topology in compact structures is not always possible. The proximity of the different resonators, assuming that these can be spatially identified, causes stray (unwanted) coupling coefficients to be present and often with comparable strength to those assumed in the selected topology.

To address this important issue, we propose to use an equivalent circuit whose form is always the same regardless of the characteristics of the response of the filter such as symmetry, presence, and number of transmission zeros at finite frequencies. It is not longer necessary to define well-localized resonances. The circuit can also model both narrow and broadband responses. In order to derive such a circuit, we start from results that are obtained directly from Maxwell's equations. The topology of the equivalent circuit is sparse, unique, and universal when the normal modes of the entire filter are used as a basis. For narrowband responses, this leads to the transversal coupling matrix, as shown in [3]. When the narrowband approximation is no longer valid, the filter can be characterized by an admittance (impedance) matrix whose form remains the same regardless of the order, symmetry, presence and number of transmission zeros at finite frequencies [3]. As long as the contribution of higher order modes to the power transport between the two ports of the filter can be ignored—this is the case for a well-designed filter with a good spurious response—a filter of order N is characterized by N resonances in or in the vicinity of its passband. When a more accurate description of the response away from the passband is needed, higher order resonances can be readily included in the equivalent circuit.

II. Two Examples

In order to better show why a new circuit model instead of the coupling matrix is needed, especially for compact filters, we consider two examples.

Manuscript received July 10, 2007; revised November 2, 2007. This work was supported in part by the Natural Science and Engineering Research Council of Canada (NSERC).

M. Bekheit is with the Department of Electrical and Computer Engineering, Queen's University, Kingston, ON, Canada K7K 5B3 (e-mail: bekheitm@ee.queensu.ca).

S. Amari is with the Department of Electrical and Computer Engineering, Royal Military College of Canada, Kingston, ON, Canada K7K 7B4 (e-mail: smain.amari@rmc.ca).

W. Menzel is with the Institute of Microwave Techniques, University of Ulm, D-89069 Ulm, Germany (e-mail: wolfgang.menzel@ieee.org).

Color versions of one or more of the figures in this paper are available online at http://ieeexplore.ieee.org.

Digital Object Identifier 10.1109/TMTT.2007.914638

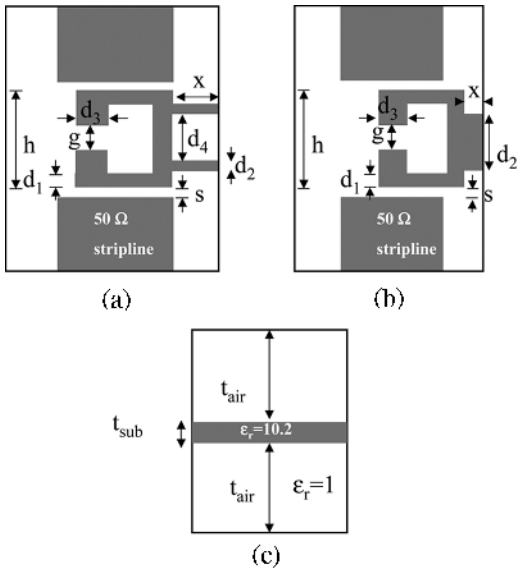

Fig. 1. (a) Layout of the second-order SSL filter with one transmission zero above the passband. (b) Layout of the second-order SSL filter with one transmission zero below the passband. (c) Cross section of the structure.

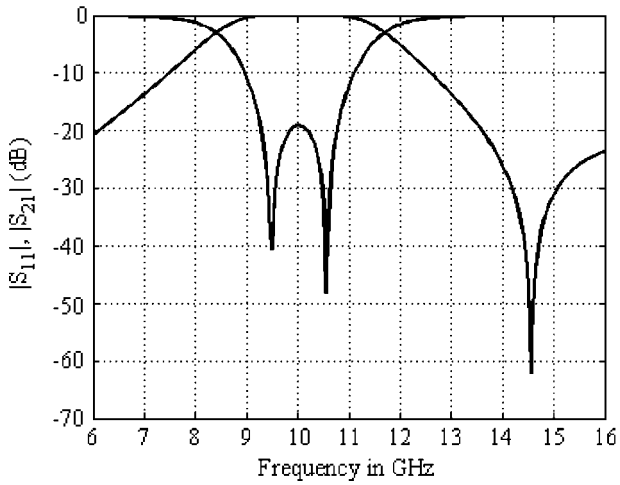

Fig. 2. Response of optimized filter in Fig. 1(a).

A. Second-Order Filter With One Transmission Zero

We first consider the second-order filters shown in Fig. 1(a) and (b). The suspended stripline (SSL) technology is chosen because it allows the implementation of compact bandpass filters with moderate to very wide bandwidths with little difficulty. Strong coupling coefficients are realized by placing the coupled elements on different sides of the suspended substrate. Weak coupling coefficients can be achieved by placing the elements on the same side [4].

The optimized response of the filter in Fig. 1(a), as obtained from the commercial software package Sonnet, is shown in Fig. 2.

In order to optimize this filter, we preferably require a simple and sparse coupling topology. The presence of the transmission zero in the upper stopband suggests the presence of cross-couplings in the structure. For example, nonzero bypass coupling between the input and the second resonator, as well as between the load and the first resonator, generates a transmission zero. Another possibility is to view the coupling between the two resonators as frequency dependent. The coupling through the gap g in Fig. 1(a) is capacitive, while the one through the portions that are grounded is inductive. The capacitive and inductive coupling paths cancel each other to generate the transmission zero [5]. It is not obvious which model is more realistic or accurate, especially when the bandwidth is increased.

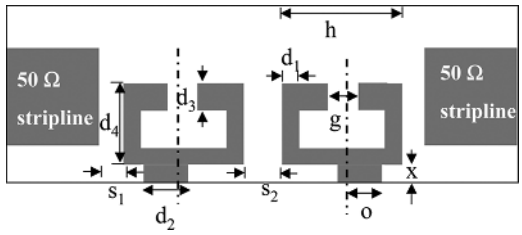

Fig. 3. Geometry of the fourth-order SSL filter.

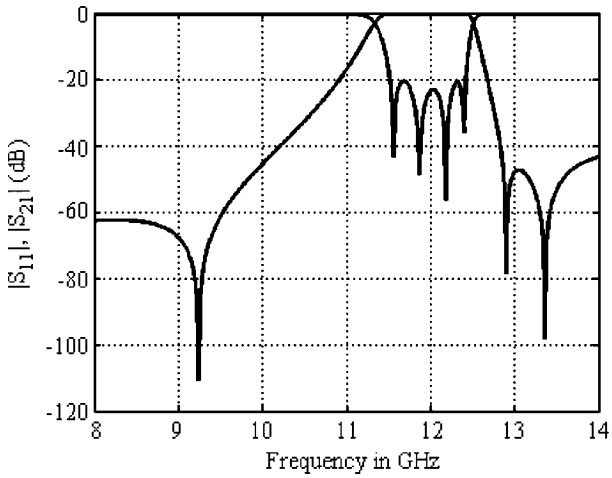

Fig. 4. Simulated response of optimized fourth-order filter with three transmission zeros.

B. Fourth-Order Filter With Three Transmission Zeros

The second example is a fourth-order bandpass filter with three transmission zeros. It is obtained by cascading two second-order building blocks of the type used in the previous example, as shown in Fig. 3. The response of this optimized filter, as obtained from Sonnet, is shown in Fig. 4.

In this seemingly inline direct-coupled resonator filter, no transmission zeros are expected to be present. The appearance of three transmission zeros suggests the presence of cross-couplings within the language of coupling matrices. Unfortunately, it is not obvious where these additional coupling paths are in the circuit. In other words, the topology of an acceptable coupling matrix yielding three transmission zeros is not readily established. As in the previous example, one might consider an equivalent circuit in which the coupling coefficients are allowed to vary with frequency. A transmission zero is generated whenever a coupling coefficient in the purely inline configuration vanishes. Unfortunately, this model would fail to predict the appearance of three distinct transmission zeros in this symmetric filter. Indeed, from symmetry considerations, the coupling coefficient

between the first and second resonators should be identical to the one between the third and last resonators. This would mean that a second-order transmission zero, instead of two distinct transmission zeros, should be observed. This is not the case.

These two examples demonstrate the limitations of using the standard coupling matrix, with a topology based on the physical arrangement of the resonators, as an equivalent circuit for both diagnosis and optimization purposes of compact microwave filters. To overcome this problem, we use a representation of the structure in which the resonances are not localized. By doing so, we eliminate the need to identify a topology since all filters will then have the same topology.

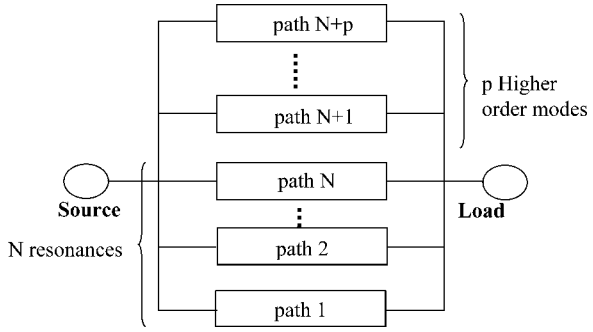

Fig. 5. Equivalent circuit of Nth-order SSL filter where N passband resonances and p higher order resonances are included.

III. Global Eigenresonance Representation of SSL Filters

In order to be able to efficiently optimize compact microwave filters, it is important to find a circuit model that accurately represents their physical behavior. The EM characteristics of cavity resonator filters are rigorously described by Maxwell's equations. A convenient approach, especially for coupled resonator filters, is to expand an arbitrary EM field in the volume of the filter in terms of the normal resonances of the entire structure. The mathematical steps and details of this formulation were reported by a number of researchers.

The first study along these lines seems to have been given by Slater who derived an expression for the input impedance of a cavity fed by a uniform waveguide [6]. Later work by Teichmann and Wigner showed that Slater failed to use a complete set of vector functions in his expansion [7]. A more detailed investigation of cavity resonators was given by Muller [8]. In a seminal paper, Kurokawa showed how the port parameters of one- and two-port cavities can be derived when complete sets of resonant solutions are used [9], [10]. Similar characteristics were discussed in connection with numerical techniques [11]–[13].

For our needs in this study, the main result is the expansion of the generalized admittance matrix of a cavity in terms of the short-circuit resonant modes. For a cavity fed by a uniform waveguide, the two-port admittance matrix takes the form [9], [10]

$$Y_{pq} = \frac{A_{pq}}{j\omega} + \sum_{i=1}^{\infty} \frac{b_{pi} b_{qi}}{j(\omega/\omega_i - \omega_i/\omega)}. \tag{1}$$

Here, $p = 1, 2$ and $q = 1, 2$ are the port numbers, A_{pq}, b_{pi}, b_{qi} are real constants related to the coupling integrals of the dominant mode in the feeding waveguide or transmission line to the ith eigenresonance in the cavity, and ω_i is the resonant angular frequency of the same resonance.

In the case of SSL filters, we assume that the structure is fed by a 50-Ω SSL, which support a quasi-TEM mode. Under these conditions, the terms $A_{pq}/j\omega$ in (1) are small enough to be neglected. For a filter of order N, we further assume that only N resonances significantly contribute to the power transport between the input and output over the frequency range of interest. If a more accurate account of the response of the filter is desired over a wider frequency band, p additional higher order resonances are retained in (1). Under these conditions, the admittance matrix in (1) reduces to

$$Y_{pq} = \sum_{i=1}^{N} \frac{b_{pi} b_{qi}}{j(\omega/\omega_i - \omega_i/\omega)} + \sum_{i=N+1}^{N+p} \frac{b_{pi} b_{qi}}{j(\omega/\omega_i - \omega_i/\omega)}. \tag{2}$$

The assumption of a quasi-TEM mode in the feeding lines implies a practically frequency-independent characteristic admittance Y_0. The inverters in (2) can be normalized by Y_0, for convenience, and remain fairly constant versus frequency. Note that, in actuality, the denormalized inverters depend only weakly on frequency since they are determined by coupling integrals, which are purely geometrical quantities for homogeneously filled structures. Although the SSL structure is not homogeneous, it is mainly the higher order modes that are significantly affected, especially for thin dielectric substrate. The SSL filters considered in this study are then described by the following admittance matrix:

$$Y_{N+p} = j \begin{bmatrix} -j & b_{11} & b_{12} & \cdots & \\ b_{11} & \dfrac{\omega}{\omega_1} - \dfrac{\omega_1}{\omega} & 0 & \cdots & b_{21} \\ b_{12} & 0 & \ddots & \cdots & \vdots \\ \vdots & 0 & \vdots & \dfrac{\omega}{\omega_{N+p}} - \dfrac{\omega_{N+p}}{\omega} & b_{2,N+p} \\ & b_{21} & \cdots & b_{2,N+p} & -j \end{bmatrix}. \tag{3}$$

Here, we again assume that N passband resonance and p higher order resonances are included. An exact circuit representation of the admittance matrix in (3) is given in Fig. 5. Each path is represented by a parallel *LC* circuit sandwiched between two admittance inverters. It is straightforward to show that the admittance parameters seen by the source and load in this circuit are identical to the expansion in (2).

To illustrate the accuracy of the equivalent circuit, the response of the second-order filter with one transmission zero, shown in Fig. 1(a), is shown in Fig. 6. The solid lines represent the full-wave simulated response as obtained from Sonnet. The dotted lines are the best fit that was obtained when only two resonances are included in the model ($N = 2$, $p = 0$). Although good agreement is achieved between the two responses in the

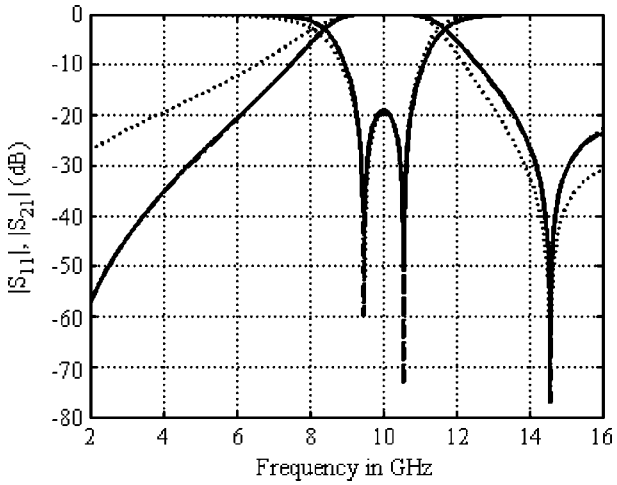

Fig. 6. Response of second-order filter with one transmission zero [see Fig. 1(a)]. Solid lines: full-wave simulation from Sonnet, dotted lines: equivalent circuit with two passband resonances ($N = 2, p = 0$) and dashed lines: equivalent circuit with two passband resonances and one higher order resonance ($N = 2, p = 1$).

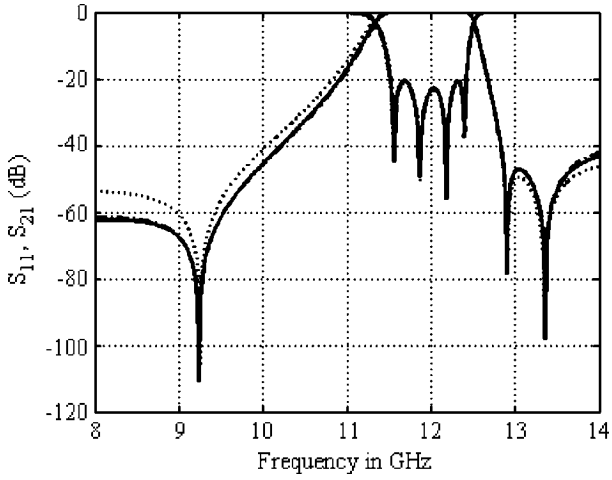

Fig. 7. Response of second-order filter with three transmission zeros (Fig. 3). Solid lines: full-wave simulation from Sonnet, dotted lines: equivalent circuit with four passband resonances ($N = 4, p = 0$) and dashed lines: equivalent circuit with four passband resonances and two higher order resonances ($N = 4, p = 2$).

passband, larger deviations appear below and above the passband. When a higher order resonance, whose resonant frequency is adjusted during the fitting process, is included, the response shown by the dashed lines is obtained. It agrees within plotting accuracy with the full-wave EM simulation. The improvement over the two-resonance circuit is evident. The circuit with one higher order resonance represents accurately the EM behavior of the filter.

Similar results are obtained for the fourth-order filter with transmission zeros whose response is shown in Fig. 4. If only four resonances, whose resonant frequencies are in the passband or its immediate vicinity, are included ($N = 4, p = 0$), the response of the corresponding equivalent circuit is shown as the dotted lines in Fig. 7. As in the previous example, good agreement is achieved in and close to the passband. The response of the equivalent circuit when four passband resonances and two higher order resonances are included ($N = 4, p = 2$) is shown as the dashed lines. It is evident that this sixth-order circuit represents accurately the EM behavior of the structure.

In order to use the equivalent circuit to optimize these filters, it is important that detuned responses be accurately approximated. As an example, the response of a detuned fourth-order filter with a relative bandwidth of roughly 20% is shown in Fig. 8. The solid lines show the simulated results as obtained from Sonnet and the dashed lines show the response of the equivalent circuit with $N = 4$ and $p = 2$. Excellent agreement between the two results is achieved.

These results show that the response of these filters can be approximated sufficiently accurately in the passband and its immediate vicinity by the equivalent circuit in Fig. 5 with only those resonances in and close to the passband included. In all cases investigated thus far, this has been sufficient to optimize the filter. When an accurate description of the response away from the passband is required, higher order resonances must be included in Fig. 5. The required number of higher order resonances is determined by the extent of the frequency range over which the response is approximated, as well as the frequency separation

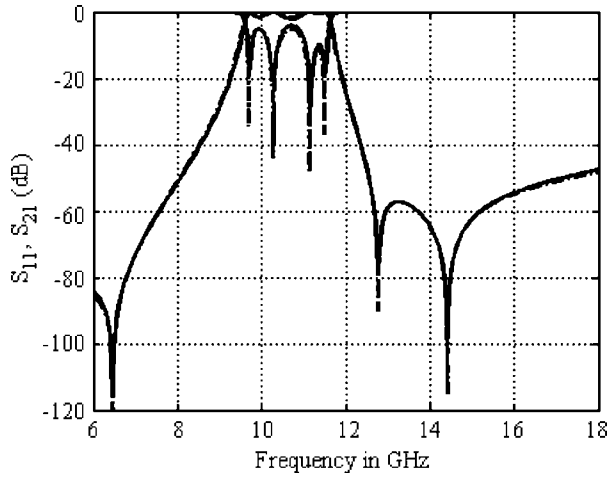

Fig. 8. Response of detuned broadband fourth order filter with three transmission zeros (Fig. 3). Solid lines: full-wave simulation from Sonnet, and dashed lines: equivalent circuit with four passband resonances and two higher order resonances ($N = 4, p = 2$).

between the edge of such a range and the next spurious band. Note that, had we insisted on using the expansion over resonant modes as a full-wave simulation tool, a much higher number of resonances would have been required to describe a lower order filter. For example, an accurate description of the response of a second-order dual-mode filter requires up to 48 modes [13, p. 195]. This number is significantly reduced by accepting not to use the expansion as a full-wave simulation tool and considering only those modes that account for the power transport, as described by the scattering parameters. In other words, we are not interested in calculating the admittance parameters in (1), as done in [13], where reference planes are placed relatively far from the first discontinuity to allow a simple extraction of the low-frequency behavior of these parameters. However, by extending the lengths of the uniform feeding lines, we introduce more modes at lower and lower resonant frequencies. On the other hand, the return loss and insertion loss of the filter are not

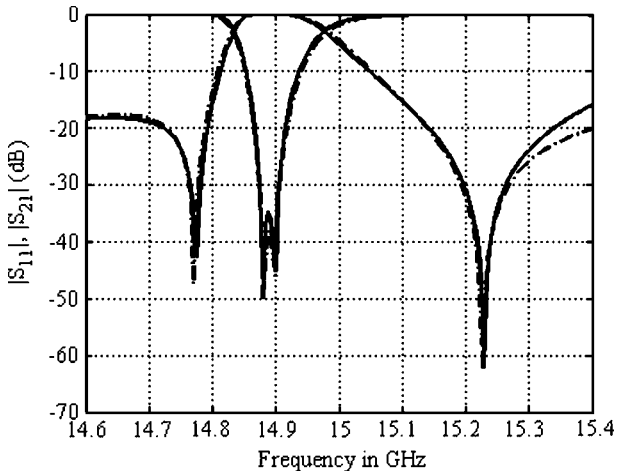

Fig. 9. Full-wave simulated response of dual-mode filter in [13] (solid lines) and response of equivalent circuit with $N = 2$ and $p = 1$ (dashed lines). The dimensions of the filter are given in [13, p. 196].

affected by the lengths of the uniform sections. It is arguably better to keep these short, ideally of zero length, thereby limiting the number of resonances in the passband and its vicinity only to those responsible for power transport. Indeed, the response of the dual-mode filter in [13] can be accurately approximated by an equivalent circuit with $N = 2$ and $p = 1$ resonances, as shown in Fig. 9. The EM simulation results, shown as solid lines, were obtained from the commercial software package μWave Wizard from Mician, Bremen, Germany. The response of the equivalent circuit, shown as the dashed lines, is in good agreement with the full-wave simulation. The slight deviation between the two results at the upper edge of the frequency range reflects the effect of other higher order resonances.

IV. Transversal Coupling Matrix

The theory presented in this paper can be used to show that the coupling matrix concept in which the coupling coefficients are assumed frequency independent is inherently narrowband. To prove this, we show that the transversal circuit used in this paper reduces to the transversal coupling matrix introduced by Cameron [14] in the narrowband limit. We start from an $(N+2)\times(N+2)$ transversal circuit whose nodal admittance matrix is of the form

$$Y = j\begin{bmatrix} -j & b_{S1} & \cdots & b_{SN} & 0 \\ b_{S1} & \dfrac{\omega}{\omega_1}-\dfrac{\omega_1}{\omega} & 0 & \cdots & b_{L1} \\ \vdots & 0 & \ddots & 0 & \vdots \\ b_{SN} & \vdots & 0 & \dfrac{\omega}{\omega_N}-\dfrac{\omega_N}{\omega} & b_{LN} \\ 0 & b_{L1} & \cdots & b_{LN} & -j \end{bmatrix}. \quad (4)$$

We define the usual normalized frequency, which describes the low-pass to bandpass transformation

$$\Omega(\omega) = \frac{\omega}{\omega_0} - \frac{\omega_0}{\omega} \quad (5)$$

where ω_0 is the center frequency of the passband. Note that the fractional bandwidth is absorbed in the normalized frequency to ease the algebra, and it can be restored at the end if needed. The transformation (5) is inverted to extract the physical frequency as

$$\omega = \frac{\omega_0}{2}(\Omega + \sqrt{\Omega^2+4}). \quad (6)$$

The negative values of ω are ignored since the passband is centered about a positive value (ω_0). In terms of Ω, the frequency-dependent diagonal elements in (4) take the form

$$\begin{aligned}\lambda_i(\Omega) &= \frac{\omega}{\omega_i} - \frac{\omega_i}{\omega} \\ &= \frac{\omega_0}{2\omega_i}(\Omega + \sqrt{\Omega^2+4}) - \frac{2\omega_i}{\omega_0}\frac{1}{\Omega+\sqrt{\Omega^2+4}}. \end{aligned} \quad (7)$$

If we expand this expression in a Taylor series around $\Omega = 0$ and keep only the first two terms, we get

$$\lambda_i(\omega) \approx \left(\frac{\omega_0}{\omega_i} - \frac{\omega_i}{\omega_0}\right) + \frac{1}{2}\left(\frac{\omega_0}{\omega_i} + \frac{\omega_i}{\omega_0}\right)\Omega = \Omega_i + a_i\Omega. \quad (8)$$

This equation is valid as long as $|\Omega|$ is small. This implies that results obtained from it are narrowband and may not be valid over a wide frequency band. The relative error in the linear approximation (8) can be easily assessed by direct comparison with (7). For example, for $\omega_1/\omega_0 = 1.2$, a 10% error results at $\Omega = 2$.

Upon substitution of (8) in (4), we get

$$Y = j\begin{bmatrix} -j & b_{S1} & \cdots & b_{SN} & 0 \\ b_{S1} & \Omega_1 + a_1\Omega & 0 & \cdots & b_{L1} \\ \vdots & 0 & \ddots & 0 & \vdots \\ b_{SN} & \vdots & 0 & \Omega_N + a_N\Omega & b_{LN} \\ 0 & b_{L1} & \cdots & b_{LN} & -j \end{bmatrix}. \quad (9)$$

Since all the a_i's defined in (8) are positive, we can scale (9) to finally get

$$Y = j\begin{bmatrix} -j & \dfrac{b_{S1}}{\sqrt{a_1}} & \cdots & \dfrac{b_{SN}}{\sqrt{a_N}} & 0 \\ \dfrac{b_{S1}}{\sqrt{a_1}} & \Omega + \dfrac{\Omega_1}{a_1} & 0 & \cdots & \dfrac{b_{L1}}{\sqrt{a_1}} \\ \vdots & 0 & \ddots & 0 & \vdots \\ \dfrac{b_{SN}}{\sqrt{a_N}} & \vdots & 0 & \Omega + \dfrac{\Omega_N}{a_N} & \dfrac{b_{LN}}{\sqrt{a_N}} \\ 0 & \dfrac{b_{L1}}{\sqrt{a_1}} & \cdots & \dfrac{b_{LN}}{\sqrt{a_N}} & -j \end{bmatrix}. \quad (10)$$

By comparing this nodal admittance matrix to that of the transversal network in [14], we can identify the transversal

coupling matrix as

$$M = \begin{bmatrix} 0 & M_{S1} & \cdots & M_{SN} & 0 \\ M_{S1} & M_{11} & 0 & \cdots & M_{L1} \\ \vdots & 0 & \ddots & 0 & \vdots \\ M_{SN} & \cdots & 0 & M_{NN} & M_{LN} \\ 0 & M_{L1} & \cdots & M_{LN} & 0 \end{bmatrix}$$

$$= \begin{bmatrix} 0 & \frac{b_{S1}}{\sqrt{a_1}} & \cdots & \frac{b_{SN}}{\sqrt{a_N}} & 0 \\ \frac{b_{S1}}{\sqrt{a_1}} & \frac{\Omega_1}{a_1} & 0 & \cdots & \frac{b_{L1}}{\sqrt{a_1}} \\ \vdots & 0 & \ddots & 0 & \vdots \\ \frac{b_{SN}}{\sqrt{a_N}} & \vdots & 0 & \frac{\Omega_N}{a_N} & \frac{b_{LN}}{\sqrt{a_N}} \\ 0 & \frac{b_{L1}}{\sqrt{a_1}} & \cdots & \frac{b_{LN}}{\sqrt{a_N}} & 0 \end{bmatrix}. \quad (11)$$

This derivation shows that the concept of the transversal coupling matrix is inherently a narrowband concept. Similarity transformations can be applied to (11) to achieve sparse topologies that are, of course, valid only for narrowband filters.

V. Optimization Examples

Here, the optimization of second- and fourth-order SSL filters is discussed. This class of filters have been reported in [15]. In this study, the operation of these filters will be modeled and explained using the global eigenmodes approach. For second-order filters, the zero-shifting property is also used to move the transmission zero from one side of the band to the other by interchanging the resonant frequencies of the even and odd modes.

The layouts of the second- and fourth-order filters are shown in Figs. 1 and 3, respectively. The thickness of the dielectric slab is $t_{\rm sub} = 0.254$ mm and the height of the air gap above and below the dielectric slab is $t_{\rm air} = 2$ mm. In some examples, the dielectric constant of the substrate is taken as $\varepsilon_r = 10.2$, whereas in others, it is $\varepsilon_r = 2.2$ when a reduced sensitivity to manufacturing errors is required. The structures are assumed lossless. The commercial software package Sonnet, in which the conducting strips are assumed of zero thickness, is used to analyze them. The optimization is based on the equivalent circuit in Fig. 5 where no higher order resonances are used. It is, however, worth mentioning that the extraction of the elements of the circuit in Fig. 5 is carried out directly in the physical frequency ω and not in the normalized low-pass frequency. In fact, no low-pass prototype is used in this study.

1) Second-Order SSL Filter: The first example is a second-order SSL filter with a fractional bandwidth of 15% and one transmission zero above the passband. The structure is shown in Fig. 1(a). Since the structure is symmetric, the frequency response of the filter can be described by its even and odd modes where the symmetry plane is at half distance between the feeding lines at the input and output. The coupling of a given mode to the input and output are also equal in magnitude. The filter is, therefore, modeled by the admittance matrix

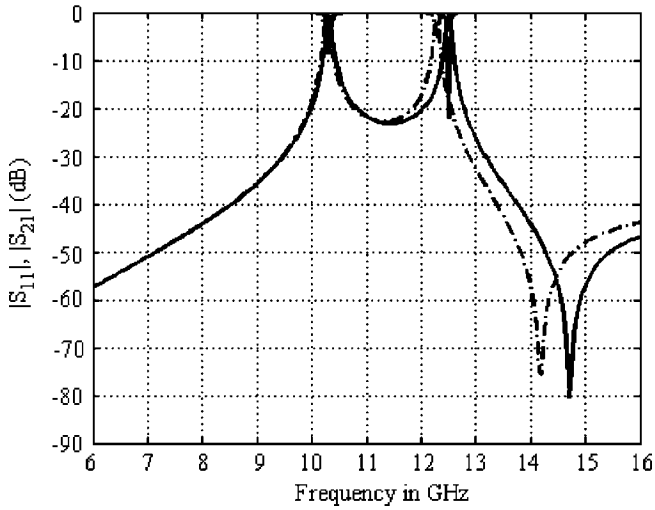

Fig. 10. EM simulated response for second-order bandpass filter with very weak input and output coupling. Solid lines: initial dimensions, dashes lines: only the g dimension is perturbed by -0.1 mm.

in (3) where only two resonances at ω_1 and ω_2 are retained, i.e.,

$$Y = j \begin{bmatrix} -j & b_{s1}\left(\frac{\omega}{\omega_1} - \frac{\omega_1}{\omega}\right) & b_{s2} & 0 \\ b_{s1}\left(\frac{\omega}{\omega_1} - \frac{\omega_1}{\omega}\right) & 0 & -b_{s1} & \\ b_{s2} & \left(\frac{\omega}{\omega_2} - \frac{\omega_2}{\omega}\right) & b_{s2} & \\ 0 & -b_{s1} & b_{s2} & -j \end{bmatrix}. \quad (12)$$

Note that the resonant frequencies ω_1 and ω_2 are not necessarily close and that the normalized inverters are assumed frequency independent, as discussed earlier.

The response of the filter can be optimized by controlling the resonant frequencies of the two modes and their respective coupling to the feeding lines. In order to control the resonant frequencies of the two modes separately, regions of strong electric and magnetic fields of each mode must be identified. A field plot can be easily generated using a field solver if needed. For example, it is obvious that the width of the gap g (see Fig. 1) impacts the resonant frequency of the mode with an electric wall along the plane of symmetry significantly more than the one with a magnetic wall. The effect of the different dimensions on the eigenmode frequencies can be investigated by weakening the coupling to the input and output (increasing s in Fig. 1) and then examining the response when a given dimension is modified. For example, when the width of the gap g is changed by -0.1 mm, the response shown in Fig. 10 is obtained. It is obvious from this figure that the width of the gap can be used to control the resonant frequency of one of the modes. Using this method, we can identify the set of dimensions that are to be perturbed in the optimization process.

The elements of the admittance matrix in (12) that yield a specified response can be determined either analytically or by optimization. For example, for a second-order filter with a center frequency of 10 GHz, in-band return loss of 20 dB, a relative bandwidth of 15%, and a transmission zero at 14.0 GHz, we obtain $b_{s1} = 0.4$, $b_{s2} = 0.271$, $\omega_1 = 8.88$ GHz, and $\omega_2 = 11.295$ GHz.

The space-mapping optimization technique is used in this study where the global eigenmode model is used as a coarse model or equivalent circuit. The technique depends on establishing a relationship between the physical dimensions and the circuit parameters (coupling and eigenmode frequencies) that can be inverted in order to calculate the target physical dimensions at every optimization step. Since the technique is well established, only a brief summary is presented here, for more details see, for example, [16] and [17].

A crucial step in this optimization technique is the extraction of the elements of the equivalent circuit. In this study, this is achieved by minimizing the following cost function:

$$K(M_1, M_2, \ldots, M_N) = \sum_{i=1}^{K} \left(\left| S_{11}^{\mathrm{EM}}(\omega_i) \right| - \left| S_{11}^{\mathrm{calc}}(\omega_i) \right| \right)^2 + \sum_{i=1}^{K} \left(\left| S_{21}^{\mathrm{EM}}(\omega_i) \right| - \left| S_{21}^{\mathrm{calc}}(\omega_i) \right| \right)^2. \tag{13}$$

Here, the circuit parameters M_i are used as optimization variables and ω_i are judiciously chosen frequency points.

A linear approximation is assumed between the circuit parameters and the physical dimensions. For a canonical problem where the number of physical dimensions is equal to the number of coarse model parameters, the Jacobian can be calculated using finite differences. Each adjustable quantity X_i is perturbed by a small, ideally infinitesimal, amount ΔX_i, and the corresponding circuit parameters extracted. After all the adjustable parameters are perturbed, we get an approximation of the Jacobian J as follows:

$$J_{ij} = \frac{\delta M_i}{\delta x_j} \cong \frac{\Delta M_i}{\Delta X_j}. \tag{14}$$

If the parameters of the equivalent circuit are grouped in a vector $[M]$ and the perturbations in a vector $[\Delta X]$, we have

$$[M] = [M_o] + [J][\Delta X] \tag{15}$$

where M_o is the vector of the initial circuit parameters (before any perturbations). The target physical dimensions can be obtained by substitution in (15) as

$$X_{\mathrm{opt}} = X_o + J^{-1} \{ [M_{\mathrm{opt}}] - [M_o] \} \tag{16}$$

where X_o is vector representing the dimensions prior to the perturbations. The process is repeated until convergence is achieved.

As an example, the second-order filter in Fig. 1(b) was designed at 10 GHz using a dielectric substrate of $\varepsilon_r = 2.2$. The initial design starts by setting the arms of the resonator to a quarter wavelength. Taking advantage of the symmetry of the structure, the even and odd modes are analyzed separately by placing electric and magnetic walls along the symmetry plane. The group delay can be obtained by means of the derivative of the phase of the reflection coefficient of the resulting one-port, as in the theory of narrowband coupled resonator filters. The controlling dimensions x and g are adjusted in order to adjust the two resonant frequencies to the required values and compensate for the loading. Initially, the dimension s is determined such that the input coupling is equal to that required for an inline filter with the same return loss. Fig. 11 shows the EM simulated response of the initial design, as obtained from the above procedure. The dimensions of this initial design are $s = 0.6$ mm, $x = 1$ mm, $g = 0.6$ mm, $d_1 = 0.8$ mm, $d_2 = 1$ mm, $d_3 = 0.9$ mm, and $h = 4.2$ mm. Note that the presence of the transmission zero is not taken into account in the initial design. Its position is adjusted first manually and then during the optimization.

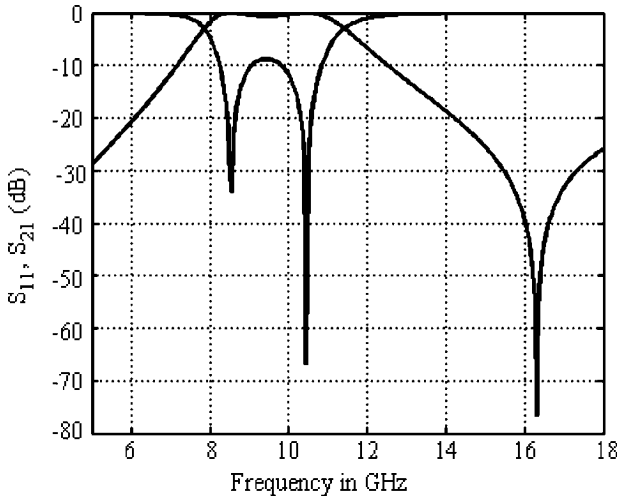

Fig. 11. Response of initial design of second-order filter. The transmission zero is not included in the design.

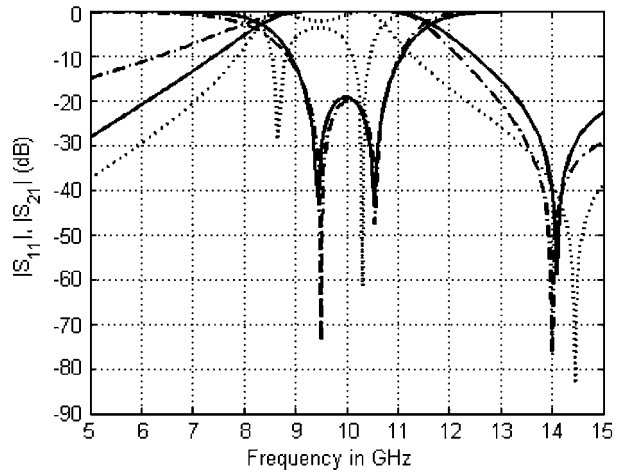

Fig. 12. Optimization progress for second-order filter starting from an extremely detuned response. Dotted line: initial response, solid line: optimized response, and dashed line: ideal response.

To better test the optimization process, the initial design was purposely detuned further, as shown by the dotted lines in Fig. 12. The progress of the optimization is shown in Fig. 12. It took three iterations to reach the response shown as the solid lines. For comparative purposes, the ideal response is shown as the dashed lines. Excellent agreement between the two curves is achieved in the passband and its vicinity. The deviation between the simulated response of the optimized structure and the ideal response away from the passband is caused by the spurious higher order reso-

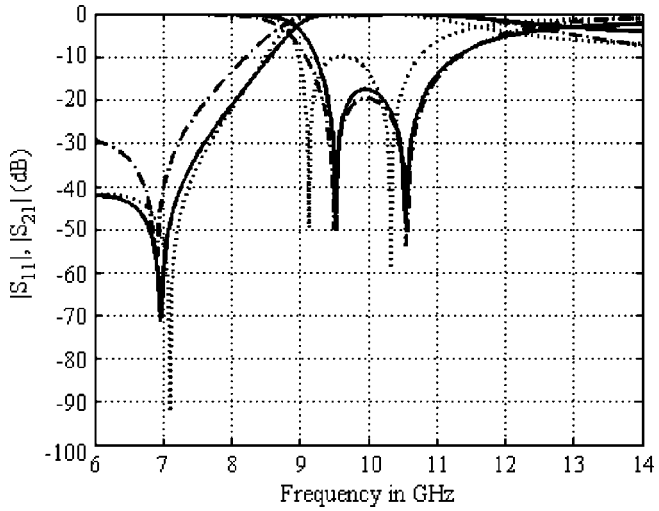

Fig. 13. Optimization progress for second-order SSL filter with transmission zero below the passband. Dotted line: initial response, solid line: optimized response (iteration 1), dotted line: ideal response.

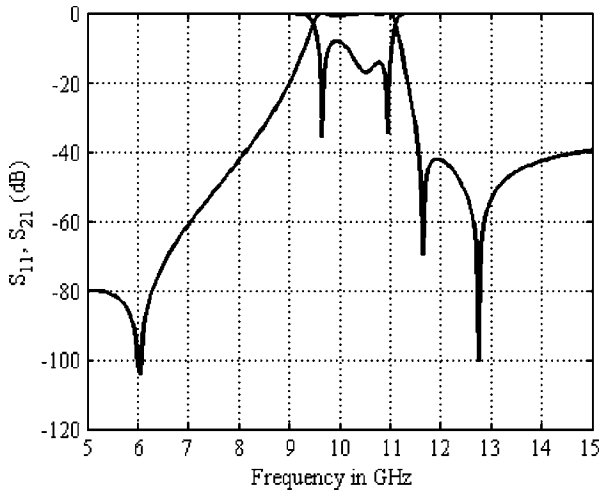

Fig. 14. Response of initial design of fourth-order filter.

nances that are not taken into account in the admittance matrix in (12) (see Fig. 6). The dimensions of the optimized filter are $s = -0.15$ mm, $x = 9.25$ mm, $g = 0.15$ mm, $d_1 = 0.8$ mm, $d_2 = 1$ mm, $d_3 = 0.9$ mm, and $h = 3.5$ mm. The negative value of the s dimension indicates that the two metallic layers, on opposite sides of the substrate, are overlapping.

A second-order filter with a transmission zero below the passband was designed based on the structure in Fig. 1(b). Compared to the filter in Fig. 1(a), the order of the resonant frequencies of the even and odd modes are reversed. This is achieved by changing the nature of the connection between the arms of the resonator and the wall of the metallic enclosure. The response of the optimized filter is shown in Fig. 13 as the solid lines. It took one iteration for the process to converge. For comparison, the ideal response is shown as the dashed lines. Good agreement between the two responses is achieved in the passband and its vicinity. As in the previous example, deviations between the two results appear away from the passband. These can be accounted for by adding higher order resonances. The dimensions of the optimized filter are $s = 0.15$ mm, $x = 0.125$ mm, $g = 0.25$ mm, $d_1 = 0.5$ mm, $d_2 = 1.8$ mm, $d_3 = 0.75$ mm, and $h = 3$ mm.

2) Fourth-Order SSL Filter: The third example is a fourth-order filter with three transmission zeros, as shown in Fig. 3. As in the previous example, in the optimization process, we only keep $N = 4$ resonances in the passband and its vicinity; all higher order resonances are "ignored" $(p = 0)$. The filter is then described by an admittance matrix of the form

$$Y = j\begin{bmatrix} -j & b_{s1} & b_{s2} & b_{s3} & b_{s4} & 0 \\ b_{s1} & \dfrac{\omega}{\omega_1}-\dfrac{\omega_1}{\omega} & 0 & 0 & 0 & -b_{s1} \\ b_{s2} & 0 & \dfrac{\omega}{\omega_2}-\dfrac{\omega_2}{\omega} & 0 & 0 & b_{s2} \\ b_{s3} & 0 & 0 & \dfrac{\omega}{\omega_3}-\dfrac{\omega_3}{\omega} & 0 & -b_{s3} \\ b_{s4} & 0 & 0 & 0 & \dfrac{\omega}{\omega_4}-\dfrac{\omega_4}{\omega} & b_{s4} \\ 0 & -b_{s1} & b_{s2} & -b_{s3} & b_{s4} & -j \end{bmatrix}. \tag{17}$$

The filter is to have a passband of 1 GHz centered at 10 GHz with an in-band return loss of 20 dB. The response must have transmission zeros at 6, 11.2, and 12.22 GHz. These specifications are met by the following values of the parameters in (17), i.e., $b_{s1} = 0.1486$, $b_{s2} = 0.2039$, $b_{s3} = 0.1767$, $b_{s4} = 0.1112$, $\omega_1 = 9.3218$ GHz, $\omega_2 = 9.7902$ GHz, $\omega_3 = 10.4123$ GHz, and $\omega_4 = 10.636$ GHz.

The initial design exploits the symmetry of the filter and a similar procedure as for the second-order filter was used. First, the length of the arms of the resonators is fixed at a quarter wavelength. Electric and magnetic walls are inserted along the symmetry plane in order to be able to analyze the even and odd modes separately. The one-port group delay can be calculated, and in this case, two peaks are observed. These occur at the eigenmode frequencies of the two even or odd modes depending on the boundary condition set at the symmetry plane. The controlling dimensions x, g, s_2, and o in Fig. 3 are adjusted such the resonant frequencies are at the required values. It should be noted that the dimension s_2 impacts the odd modes more than the even ones; it can be fixed in the configuration with the electric wall along the symmetry plane. Fig. 14 shows the response of the initial design. The corresponding dimensions are $s_1 = 0$, $s_2 = 0.6$ mm, $x = 0.7$ mm, $o = 0.4$ mm, $g = 0.2$ mm, $h = 4.2$ mm, $d_1 = 0.8$ mm, $d_2 = 1$ mm, $d_3 = 0.9$ mm, and $d_4 = 3.3$ mm. Note that the transmission zero are not included in the initial design. Their positions is first adjusted manually and then during the optimization process.

The progress of the optimization process is shown in Fig. 15 along with the ideal response as obtained from the nodal admittance matrix in (17). One iteration based on a linear approximation [17] is sufficient to bring the in-band return loss from 11 to 20 dB and adjust the bandwidth and center frequency of the passband. A dielectric slab with $\varepsilon_r = 2.2$ is used where the input lines and the resonators are placed on opposite sides of the substrate. The six controlling dimensions that were perturbed and optimized are s_1, s_2, x, o, g, and h (see Fig. 3). The dimensions of the optimized filter are $s_1 = 0.0625$ mm, $s_2 = 0.825$ mm, $x = 0.65$ mm, $o = 0.325$ mm, $g = 0.325$ mm, $h = 4.65$ mm, $d_1 = 0.8$ mm, $d_2 = 1$ mm, $d_3 = 0.95$ mm, and

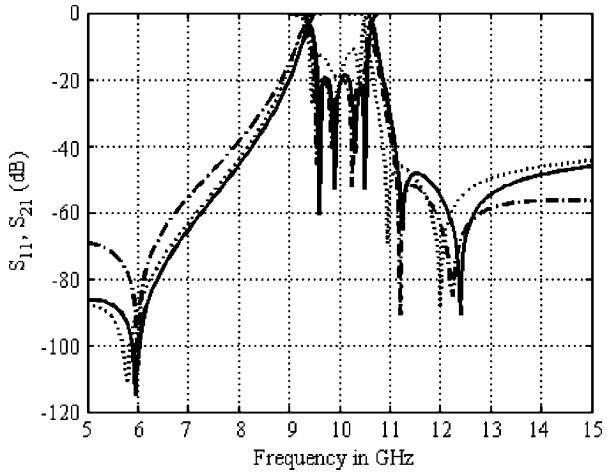

Fig. 15. Optimization progress for fourth-order SSL filter. Dotted lines: initial response, solid lines: optimized response (one iteration), dashed lines: ideal response.

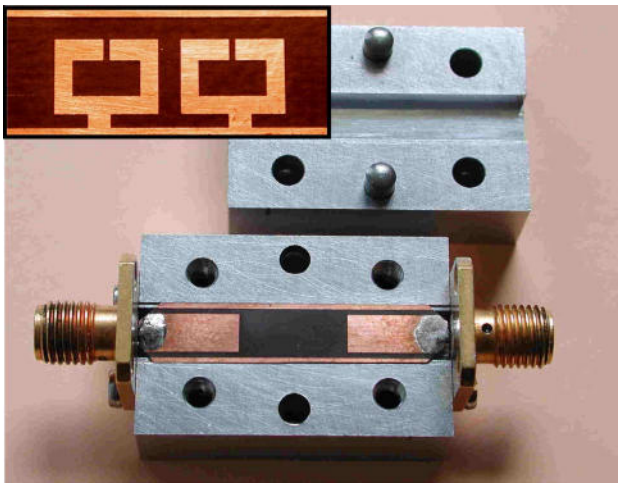

Fig. 16. Fabricated fourth-order filter with opened metallic enclosure and feeding lines. The four resonators on the backside of the substrate are shown in the inset (not to scale) of this figure.

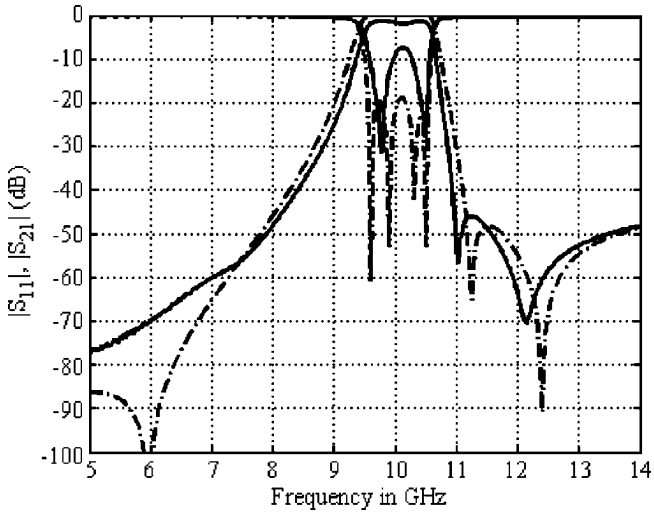

Fig. 17. Measured (solid lines) and simulated (dashed lines) results of fourth-order filter.

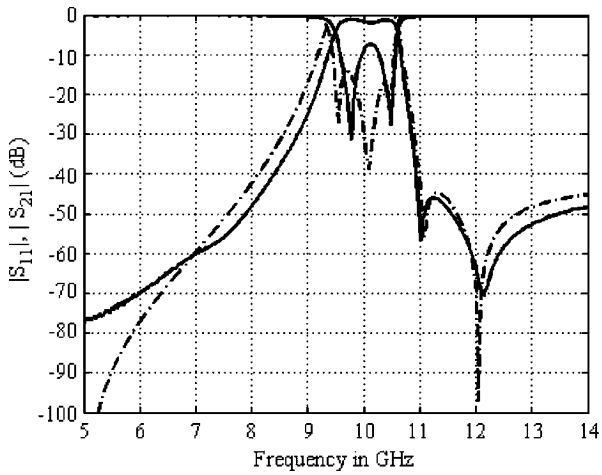

Fig. 18. Measured (solid lines) and simulated (dashed lines) results of the structure that was actually fabricated.

$d_4 = 3.35$ mm. Although a total of eight parameters are needed to adjust the structure to yield an arbitrary fourth-order response with three transmission zeros, the selected six parameters were sufficient to meet the specifications. For more general and arbitrary requirements, more adjustable parameters may be needed. In such a case, the concept of pseudoinverse or singular value decomposition can be used to obtained the best set of values of the parameters at each iteration. A minimization approach can also be used to determine the optimal values of the parameters at each iteration.

VI. Experimental Results

A fourth-order filter with three transmission zeros was selected for fabrication. Given the sensitive nature of these filters, a lower dielectric constant of $\varepsilon_r = 2.2$ was chosen in order to reduce the effect of manufacturing errors. The other dimensions of the metallic enclosure remain unchanged from Fig. 1. The filter was optimized by following the same procedure as in the previous example.

A photograph of the fabricated filter is shown in Fig. 16. The measured and simulated results are shown in Fig. 17 as the solid and dashed lines, respectively. Acceptable agreement is achieved between the simulated and measured insertion loss of the filter. Deviations between the in-band return loss reflect the sensitivity of these types of filters to manufacturing errors and the mismatch caused by the SMA connectors at the input and output. Better agreement between the simulated and measured results is obtained when the small extension of the dielectric layer into grooves to suspend it is included in the simulation process.

The fabricated substrate is placed into a 30-mm-long mount and soldered to coaxial connectors. Substrate edges were cut slightly to improve the return loss of the transitions. Measurements were done with an Agilent 8510 network analyzer using a coaxial two-port calibration. Accordingly, the measured results include some excess line length and the transitions to the coaxial measurement system.

A comparison between the measured and simulated results with the modifications in place is shown in Fig. 18. Compared

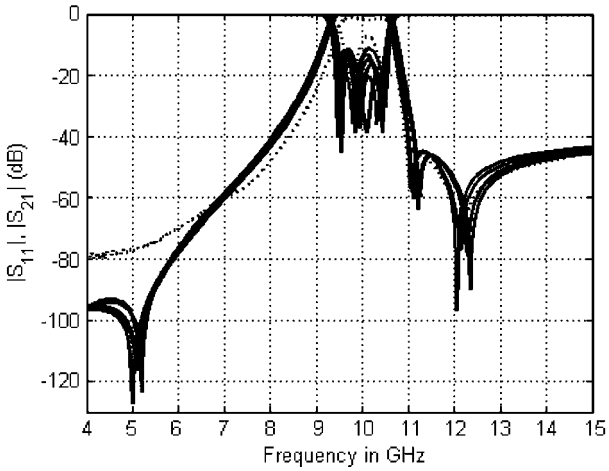

Fig. 19. Sensitivity analysis of the fabricated structure. Only the dimensions s_1, g, and x are varied by ± 25 μm each. Solid line: EM simulations and dotted line: measurements.

to Fig. 17, better agreement is achieved. Fig. 19 shows the sensitivity analysis of the fabricated structure when only three dimensions (s_1, g, and x) were allowed to vary by ± 25 μm each. It is obvious from the plot that the filter is quite sensitive to manufacturing tolerances, especially in the passband where the return loss falls to 11 dB when the three dimensions are perturbed simultaneously. In this analysis, metallic and dielectric losses were not taken into consideration. The remaining difference between the measured and simulated return loss (roughly 3 dB) may be due to losses and the SMA transitions, which are not taken into account in the simulation.

VII. Conclusions

A technique that exploits an equivalent circuit based on the global eigenmodes of the entire filter, instead of the individual resonators, as used in coupled-resonator filter theory, has been used to optimize compact bandpass microwave filters. The equivalent circuit overcomes the difficult issue of identifying a simple and sparse topology in compact structures where stray couplings are too strong to neglect. Within the presented approach, the form of the admittance (impedance) matrix representing the filter is always the same regardless of the characteristics of the response of the filter. The equivalent circuit has the advantage of handling narrowband, as well as broader bandwidths. Broadband filters can be modeled by including the global eigenmodes whose resonant frequencies fall within or close to the passband, as well as few higher order modes. The technique has been applied to the optimization of filters with bandwidths of up to 15%. Good results have been obtained.

References

[1] A. E. Atia and A. E. Williams, "New types of bandpass filters for satellite transponders," *COMSAT Tech. Rev.*, vol. 1, pp. 21–43, Fall, 1971.

[2] F. Seyfert, L. Baratchart, J. P. Marmorat, S. Bila, and J. Sombrin, "Extraction of coupling parameters for microwave filters: Determination of a stable rational model from scattering data," in *IEEE MTT-S Int. Microw. Symp Dig.*, Philadelphia, PA, Jun. 2003, pp. 24–28.

[3] S. Amari and M. Bekheit, "Physical interpretation and implications of similarity transformations in coupled resonator filter design," *IEEE Trans. Microw. Theory Tech.*, vol. 55, no. 6, pp. 1139–1153, Jun. 2007.

[4] W. Menzel and A. Belalem, "Quasi-lumped suspended substrate filters and diplexers," *IEEE Trans. Microw. Theory Tech.*, vol. 53, no. 10, pp. 3230–3237, Oct. 2005.

[5] W. Menzel and M. Berry, "Quasi-lumped suspended stripline filters with adjustable transmission zeroes," in *IEEE MTT-S Int. Microw. Symp. Dig.*, 2004, vol. 1, pp. 375–378.

[6] J. C. Slater, *Microwave Electronics*. New York: Van Nostrand, 1950.

[7] T. Teichmann and E. P. Wigner, "Electromagnetic field expansion in loss-free cavities excited through holes," *J. Appl. Phys.*, vol. 24, pp. 262–267, Mar. 1957.

[8] R. Muller, "Theory of cavity resonators," in *Electromagnetic Waveguides and Cavities*, G. Goubeau, Ed. New York: Pergamon, 1961, ch. 2.2.

[9] K. Kurokawa, "The expansion of electromagnetic fields in cavities," *IRE Trans. Microw. Theory Tech.*, vol. MTT-6, no. 4, pp. 178–187, Apr. 1958.

[10] K. Kurokawa, *An Introduction to the Theory of Microwave Circuits*. New York: Academic, 1969.

[11] T. Okoshi, *Planar Circuits for Microwaves and Lightwaves*. New York: Springer-Verlag, 1985.

[12] M. Dohlus, R. Schuhmann, and T. Weiland, "Calculation of frequency domain parameters using 3-D eigensolutions," *Int. J. Numer. Modeling*, vol. 12, pp. 41–68, 1999.

[13] G. Conciauro, M. Guglielmi, and R. Sorrentino, *Advanced Modal Analysis*. New York: Wiley, 2000.

[14] R. J. Cameron, "Advanced coupling matrix synthesis techniques for microwave filters," *IEEE Trans. Microw. Theory Tech.*, vol. 50, no. 1, pp. 1–10, Jan. 2003.

[15] A. Balalem, W. Menzel, and A. Omar, "Quasi-lumped-open loop suspended stripline bandpass filter," in *Eur. Microw. Conf.*, Manchester, U.K., Sep. 2006, pp. 568–571.

[16] J. W. Bandler, Q. S. Cheng, S. A. Dakroury, A. S. Mohamed, M. H. Bakr, K. Madsen, and J. Sondergaard, "Space mapping: The state of the art," *IEEE Trans. Microw. Theory Tech.*, vol. 52, no. 1, pp. 337–361, Jan. 2004.

[17] S. Amari, C. LeDrew, and W. Menzel, "Space mapping optimization of planar coupled resonators filters," *IEEE Trans. Microw. Theory Tech.*, vol. 54, no. 5, pp. 2153–2159, May 2006.

Maged Bekheit (M'03) received the B.Sc. degree from Ain Shams University, Cairo, Egypt, in 1999, the M.Sc. degree from Queen's University, Kingston, ON, Canada, in 2005, and is currently working toward the Ph.D. degree at Queen's University.

Since 1999, he has been an RF Planning and Optimization Engineer with a number of cellular companies. His research is focused on the design and optimization techniques of microwave components.

Mr. Bekheit was the recipient of the Natural Sciences and Engineering Council (NSERC) of Canada Graduate Scholarship (CGS) and an Ontario Graduate Scholarship (OGS) Award.

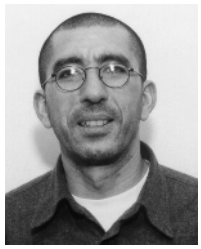

Smain Amari (M'98) received the DES degree in physics and electronics from Constantine University, Constantine, Algeria, in 1985, and the Masters degree in electrical engineering and Ph.D. degree in physics from Washington University, St. Louis, MO, in 1989 and 1994, respectively.

From 1994 to 2000, he was with the Department of Electrical and Computer Engineering, University of Victoria, Victoria, BC, Canada. From 1997 to 1999, he was a Visiting Scientist with the Swiss Federal Institute of Technology, Zurich, Switzerland, and a Visiting Professor in Summer 2001. In 2006. he was a Visiting Professor with the University of Ulm, Ulm, Germany. Since November 2000, he has been with the Department of Electrical and Computer Engineering, Royal Military College of Canada, Kingston, ON, Canada, where he is currently a Professor. His research interests are numerical analysis, numerical techniques in electromagnetics, applied physics, applied mathematics, wireless and optical communications, computer-aided design (CAD) of microwave components, and application of quantum field theory in quantum many-particle systems.

Wolfgang Menzel (F'01) received the Dipl.-Ing. degree in electrical engineering from the Technical University of Aachen, Aachen, Germany, in 1974, and the Dr.-Ing. degree from the University of Duisburg, Duisburg, Germany, in 1977.

From 1979 to 1989, he was with the Millimeter-Wave Department, AEG, Ulm, Germany [now the European Aerospace, Defense, and Space Systems (EADS)]. From 1980 to 1985, he was Head of the Laboratory for Integrated Millimeter-Wave Circuits, AEG. From 1985 to 1989, he was Head of the entire Millimeter-Wave Department, AEG. During that time, his areas of interest included planar integrated circuits (mainly on the basis of fin-line techniques), planar antennas, and systems in the millimeter-wave frequency range. In 1989, he became a Full Professor with the Institute of Microwave Techniques, University of Ulm, Ulm, Germany. His current areas of interest are multilayer planar circuits, waveguide filters and components, antennas, millimeter-wave and microwave interconnects and packaging, and millimeter-wave application and system aspects.

Dr. Menzel was an associate editor for the IEEE TRANSACTIONS ON MICROWAVE THEORY AND TECHNIQUES (2003–2005). From 1997 to 1999, he was a Distinguished Microwave Lecturer for Microwave/Millimeter Wave Packaging. From 1997 to 2001, he chaired the German IEEE Microwave Theory and Techniques (MTT)/Antennas and Propagation (AP) Chapter. He was the recipient of the 2002 European Microwave Prize.